NeuroImage 63 (2012) 1353–1363

Contents lists available at SciVerse ScienceDirect

NeuroImage

journal homepage: www.elsevier.com/locate/ynimg

Absolute quantification of resting oxygen metabolism and metabolic reactivity during functional activation using QUO2 MRI

C.J. Gauthier [a,b,*], L. Desjardins-Crépeau [b,c], C. Madjar [b], L. Bherer [b,c], R.D. Hoge [a,b]

[a] Physiology/Biomedical Engineering, Université de Montréal, Montreal, Quebec, Canada
[b] CRIUGM, Montreal, Quebec, Canada
[c] UQAM, Psychology Department, Montreal, Quebec, Canada

ARTICLE INFO

Article history:
Accepted 23 July 2012
Available online 16 August 2012

Keywords:
Calibrated fMRI
Baseline oxygen use
Evoked oxidative metabolism
Stroop task
Hypercapnia
Hyperoxia

ABSTRACT

We have recently described an extension of calibrated MRI, which we term QUO2 (for QUantitative O_2 imaging), providing absolute quantification of resting oxidative metabolism ($CMRO_2$) and oxygen extraction fraction (OEF_0). By combining BOLD, arterial spin labeling (ASL) and end-tidal O_2 measurements in response to hypercapnia, hyperoxia and combined hyperoxia/hypercapnia manipulations, and the same MRI measurements during a task, a comprehensive set of vascular and metabolic measurements can be obtained using a generalized calibration model (GCM). These include the baseline absolute CBF in units of ml/100 g/min, cerebrovascular reactivity (CVR) in units of %Δ CBF/mm Hg, M in units of percent, OEF_0 and $CMRO_2$ at rest in units of μmol/100 g/min, percent evoked $CMRO_2$ during the task and n, the value for flow-metabolic coupling associated with the task. The M parameter is a calibration constant corresponding to the maximal BOLD signal that would occur upon removal of all deoxyhemoglobin. We have previously shown that the GCM provides estimates of the above resting parameters in grey matter that are in excellent agreement with literature. Here we demonstrate the method using functionally-defined regions-of-interest in the context of an activation study. We applied the method under high and low signal-to-noise conditions, corresponding respectively to a robust visual stimulus and a modified Stroop task. The estimates fall within the physiological range of literature values, showing the general validity of the GCM approach to yield non-invasively an extensive array of relevant vascular and metabolic parameters.

Introduction

Blood oxygen-level dependent (BOLD) fMRI has been used extensively since its discovery to investigate non-invasively the brain activity associated with a large variety of tasks. Though BOLD contrast is a sensitive measure of activity, it is unfortunately also an ambiguous one, as it arises from a combination of changes in oxidative metabolism, blood flow and blood volume. Calibrated fMRI techniques were developed to isolate the oxidative metabolic component of the BOLD signal, a quantity thought to better reflect the underlying synaptic activity of neurons. These techniques use gas manipulations such as hypercapnia (Davis et al., 1998; Hoge et al., 1999), hyperoxia (Chiarelli et al., 2007) or a combination of both (Gauthier and Hoge, in press-a) to estimate the purely vascular component of the BOLD response and remove it from the BOLD signal measured during a task. The resulting estimate of percent cerebral metabolic rate of O_2 ($CMRO_2$) change evoked by that specific task can then be directly compared between groups, even if these groups are known to differ in their hemodynamic function.

The importance of the baseline state in understanding the meaning of vascular and metabolic dynamic changes is becoming more and more appreciated. Task-induced BOLD signal changes cannot, in standard fMRI protocols, be related to a known baseline state. This reduces the strength of inferences that can be made about the signal changes measured, since not only are these BOLD changes ambiguous physiologically, but they are expressed as a function of an unknown baseline with an unknown inter-subject and inter-group variability. Until recently, calibrated fMRI studies have suffered from a related weakness in that even though the actual percent changes in $CMRO_2$ have a physiological meaning that allows direct group comparisons, these percent changes arise from an unknown baseline, thereby limiting the conclusions that may be drawn from the observation of group differences.

Efforts to characterize the resting state of the brain have led to the development of a number of new imaging and analysis techniques for the measurement of baseline metabolism (Bolar et al., 2011a; Bulte et al., 2011; Fan et al., 2011; He and Yablonskiy, 2007; He et al., 2008). We have recently proposed an extension of our Generalized calibration model (GCM) technique (Gauthier and Hoge, in press-a) that takes

* Corresponding author at: 4565 Queen Mary, M6803, Montreal, Qc, H3W 1W5, Canada. Fax: +1 514 340 3548.
E-mail address: claudine.gauthier@umontreal.ca (C.J. Gauthier).

1053-8119/$ – see front matter © 2012 Elsevier Inc. All rights reserved.
http://dx.doi.org/10.1016/j.neuroimage.2012.07.065

advantage of the common and orthogonal information contained in the MRI and end-tidal partial pressure of expired O_2 (ETO_2) measured in response to different combinations of hypercapnia and hyperoxia to get an estimate of baseline properties including M, the oxygen extraction fraction at rest (OEF_0) and oxidative metabolism at rest ($CMRO_2$) in micromolar units (Gauthier and Hoge, in press-b). The parameter M corresponds to the BOLD signal attenuation at rest from baseline deoxyhemolobin content and is used in calibrated fMRI experiments to calibrate task-evoked BOLD signal changes. It is estimated using a BOLD biophysical model by extrapolation from the signal changes observed during gas manipulations to the maximal possible BOLD signal increase that would theoretically occur upon complete removal of deoxyhemoglobin. The technique to measure baseline properties (Gauthier and Hoge, in press-b), combined with the established calibrated fMRI of task-evoked metabolism, provides a rich array of vascular and metabolic parameters including measures of oxygen delivery, resting cerebral blood flow, CO_2-mediated cerebrovascular reactivity, the resting BOLD signal M, flow-metabolic coupling, as well as both absolute measures of baseline and task-evoked oxidative metabolism. This approach, which we have dubbed QUO2 MRI (for QUantitative O_2), could be of great value in the interpretation of basic neuroscience research results, but also in the investigation of complex diseases that include functional and hemodynamic deficits.

Here we present the framework by which these different aspects of the model can be combined to characterize the brain vasculature and metabolism using two widely used paradigms: intense stimulation of primary visual areas using a flashing checkerboard and a modified version of the Stroop task, producing much more subtle brain responses. New functional imaging techniques are often tested using simple visual paradigms, since these tasks represent a best case scenario for functional imaging, giving rise to well characterized, very large signal changes readily observable even with low signal-to-noise ratio (SNR) techniques. While this provides a good proof-of-concept framework for testing new techniques, cognitive tasks used in basic neuropsychology and clinical settings typically produce much smaller responses and are thus more challenging to image than primary sensory stimulation. The modified Stroop task (Bohnen et al., 1992) used here includes both an inhibition and a task switching component. This makes this task interesting for an in-depth study of local physiology since these executive functions have been shown to be specifically affected by aging and some diseases (Milham et al., 2002; Wasylyshyn et al., 2011; Yun et al., 2011). It is therefore possible that the regions implicated in these tasks show signs of a more fragile underlying physiology that would explain their vulnerability to age and disease.

Methods

Acquisitions were conducted in seven healthy male subjects (aged 21 to 38 years) on a Siemens TIM Trio 3T MRI system (Siemens Medical Solutions, Erlangen, Germany) using the vendor-supplied 32-channel receive-only head coil for all acquisitions. All subjects gave informed consent and the project was approved by the Comité mixte d'éthique de la recherche du Regroupement Neuroimagerie/Québec.

Image acquisition

Sessions included an anatomical, 1 mm^3 MPRAGE acquisition with TR/TE/alpha = 2300 ms/3 ms/9°, 256×240 matrix and a GRAPPA acceleration factor of 2 (Griswold et al., 2002).

Functional image series were acquired using a dual-echo pseudo-continuous arterial spin labeling (pCASL) acquisition (Wu et al., 2007) to measure changes in cerebral blood flow (CBF). The parameters used include: TR/TE1/TE2/alpha = 3000 ms/10 ms/30 ms/90° with 4×4 mm in-plane resolution and 11 slices of 7 mm (1 mm slice gap) on a 64×64 matrix (at 7/8 partial Fourier), GRAPPA acceleration factor = 2, post-labeling delay = 900 ms, label offset = 100 mm, Hanning window-shaped RF pulse with duration/space = 500 μs/360 μs, flip angle of labeling pulse = 25°, slice-selective gradient = 6 mT/m, tagging duration = 1.5 s (Wu et al., 2007).

Gas manipulations

Each session included three functional runs each including a different gas manipulation. During each gas manipulation run, a single three-minute block of gas inhalation was preceded with 1 min and followed by 2 min of medical air breathing. The three gas manipulations used were: 100% O_2 (hyperoxia), 7% CO_2/21%O_2/72%N_2 (hypercapnia) and 7% CO_2/93% O_2 (simultaneous hyperoxia/hypercapnia). The latter gas is a specific formulation of carbogen, which in general may contain different O_2/CO_2 ratios.

At the beginning of the experiment, subjects were fitted with a non-rebreathing face mask (Hudson RCI, #1059, Temecula, California, USA). To avoid discomfort from outward gas leakage blowing into the subject's eyes, skin tape (Tegaderm Film, #1626W, 3M Health Care, St-Paul, MN, USA) was used to seal the top of the mask to the face. Plastic tubing (AirlifeTM Oxygen tubing #001305, Cardinal Health, McGraw Park, IL, USA) and a series of two Y-connectors were used to connect pressure/flow-meters for medical air, 100% O_2 (hyperoxia), 7% CO_2/93% air (hypercapnia) and 7% CO_2/93% O_2 (simultaneous hyperoxia/hypercapnia) tanks (Vitalaire, Mississauga, ON, Canada) to the mask. Gas flows were adjusted manually on the pressure/flow-meters (MEGS, Ville St-Laurent, QC, Canada) to keep a total flow rate of 16 L/min. Gas flow was kept at 16 L/min at all times except during administration of the hyperoxia/hypercapnia and the hypercapnia gas mixtures. To accommodate the elevated minute ventilation caused by CO_2 breathing, gas flow rates were increased to the maximal possible rate (25 L/min) achievable with our pressure/flowmeters. Pulse rate and arterial O_2 saturation were monitored in all subjects using a pulse-oximeter (InVivo Instruments, Orlando, USA) as a safety measure and to observe the effects of the different gas manipulations.

End-tidal O_2 and CO_2 values were monitored during all acquisitions. Gases were sampled via an indwelling (15 mm) nasal cannula (AirlifeTM Nasal Oxygen Cannula #001321, Cardinal Health, McGraw Park, IL, USA) using the CO2100C and O2100C modules of the MP150 BIOPAC physiological monitoring unit (BIOPAC Systems Inc., Goleta, CA, USA). Calibration of the unit was done by taking into account an expired partial pressure of water of 47 mm Hg (Severinghaus, 1989). Subjects were instructed to breathe through their nose, which ensured that only expired gas was sampled by the nasal cannula. End-tidal PCO_2 and PO_2 values were selected manually from continuous respiratory traces sampled at 200 Hz. The first 10 breaths of the first baseline period and the last 10 breaths of the gas-inhalation block were averaged to give baseline values and gas manipulation values respectively.

After the experiment, all subjects were debriefed to assess the level of discomfort associated with the breathing manipulations. The subjects were asked to rate the air hunger and breathing discomfort associated with the hypercapnia and carbogen mixtures on a French language version of the scale proposed in (Banzett et al., 1996).

Visual stimulus

The visual stimulus used was a black and white radial checkerboard, with annuli scaled logarithmically with eccentricity, luminance modulated in a temporal squarewave at 8 Hz (equivalent to 16 contrast reversals per second) presented using an LCD projector (EMP-8300, Epson, Toronto, ON, Canada) onto a translucent screen viewed by subjects through a mirror integrated into the Siemens head coil. This stimulation was initiated 1 min into the acquisition and lasted 3 min, followed by 2 min of rest.

Stroop task

The Stroop task consisted of two 60-second blocks each of control and Stroop conditions, interspersed with 60-second rest blocks. In total, there were therefore four task and five resting blocks, for an acquisition of 9 min. During task blocks, control or Stroop events always lasted 2 s, preceded by 2 s with a fixation cross to maintain focus. In all cases, subjects had only two possible answers (blue or green), selected using an MRI-compatible button box (FIU-005 interface with 8 buttons bimanual response pads, Current Designs). All subjects were native French speakers and the color words were written in French ('BLEU' and 'VERT'). The task was presented to the participant using the same setup as for the visual task.

During the Stroop/switching condition blocks, two different types of events were given in random order. In all cases, letter color and word semantic were non-congruent. In ten of fifteen cases, when the color word appeared, the correct answer was letter color. In five cases out of fifteen, a large white rectangle appeared around the word for the whole event, starting during the 2 s with the fixation cross. This rectangle indicated to the subject that the rule had changed and that the right answer now corresponded to word semantic rather than letter color. During the control task blocks (color naming), a series of four X's were written either in blue or green and the participant was asked to give the color of the letters.

Data analysis

All analyses except for Stroop ROIs definition were done using the NeuroLens data analysis software package (www.neurolens.org). The raw EPI series were preprocessed by motion correction (Cox and Jesmanowicz, 1999) and spatial smoothing with a 3D Gaussian kernel (6 mm FWHM). The CBF signal was isolated from the series of first echoes using linear surround subtraction (Liu and Wong, 2005), while the BOLD signal was extracted using linear surround addition of the second echo series.

Fractional changes in BOLD and CBF signals were then determined for each gas manipulation by fitting a GLM to the respective signals and dividing the estimated effect size by the estimated constant term. Model fits used a single-gamma hemodynamic response function (HRF) with parameters described by Glover (1999) and included a first order polynomial to represent baseline signal and linear drift (higher order polynomial fits were deemed unsuitable due to the single long block during the gas runs). Because the canonical HRF cited above actually bears little resemblance to the impulse response describing transitions between respiratory states, the first 60 s after each transition in gas composition were excluded from the analyses by zeroing out relevant rows in the GLM computational matrices, to select responses at steady-state. CBF and BOLD data for the visual and Stroop tasks were treated similarly, but no frames were excluded. For the Stroop task, a third order drift polynomial was used in the GLM and a contrast was used to isolate the signal changes during the Stroop/switching blocks.

Because the flow changes produced by hyperoxia were considerably smaller than the noise level in our ASL acquisitions, a constant fixed value of −3.11% was assumed for this CBF change (only for hyperoxia). This value was the average flow change determined by first averaging the O_2-induced change in ASL signal (after correction for T1 changes as described below) over all cortical and sub-cortical grey matter in each subject, and then pooling average values from the seven subjects. The use of a fixed value for the O_2-induced flow response is also advocated in the Chiarelli method (Chiarelli et al., 2007), as these changes are generally agreed to be too small for reliable measurement at the single voxel level with current ASL methods.

As noted above, it was necessary to correct values of the fractional CBF change during hyperoxic manipulations to account for changes in the T1 of blood known to occur during changes in the plasma concentration of O_2 (which is paramagnetic). This was carried out using the approach described in Chalela et al. (2000); Zaharchuk et al. (2008). We estimated arterial blood T1 values based on the end-tidal O_2 (ETO_2) measurements obtained in each subject, along with T1 vs. FiO_2 values tabulated in Bulte et al. (2007) and PaO_2 vs. FiO_2 values tabulated by Chiarelli et al. (2007). Since the exact T1 depends on the level of dissolved O_2 in plasma, and because we obtained slightly different ETO_2 values at a given fraction of inspired O_2 than in these studies because of differences in gas delivery techniques, the values were linearly interpolated to account for this difference.

Following determination of average end-tidal O_2 values as described above, the latter were converted to arterial O_2 content in ml O_2/ml blood as described in Chiarelli et al. (2007). The following parameters were assumed for all subjects in the latter conversion: $\varphi = 1.34$ mlO_2/gHb, [Hb] = 15 gHb/dl blood, and $\varepsilon = 0.0031$ mlO_2/dl blood/mm Hg (the solubility of O_2 in plasma) (Chiarelli et al., 2007; Rhoades and Bell, 2009). While hemoglobin concentration was assumed here to be 15 gHb/dl blood, this value can be determined more accurately through a blood draw for each subject. Two of our participants underwent this test as part of another study and their blood hemoglobin concentrations were 14.5 and 15.2 gHb/dl blood, close to the assumed value of 15 gHb/dl blood.

For the three gas manipulations, the corresponding fractional changes in BOLD and CBF along with arterial O_2 content values were substituted into the generalized calibration model to determine the M vs. OEF_0 curve for each gas (the averaging performed on the measured MRI and respiratory values is described below). The intersection point of the two curves was then determined numerically using the bisection method (Press et al., 1992), starting from an OEF_0 value of 1. The midpoint between the intersection between the hypercapnia (HC) and hyperoxia (HO) curves and the intersection point between the combined hyperoxia/hypercapnia (HO-HC) and hyperoxia (HO) curves was used to determine the M vs. OEF_0 solution coordinates used in further analyses.

Computation of resting $CMRO_2$ required the absolute resting CBF, which was determined from the pCASL data using the approach described by Wang et al. (2003) assuming blood brain partition coefficient = 0.9, labeling efficiency = 0.80, blood T1 = 1.49 s, and grey matter T1 = 1.4 s. For this computation, the baseline ASL difference signal estimated in the GLM fit for each gas manipulation was divided by an estimate of the baseline (raw) EPI signal computed in a similar GLM fit. The resultant ratio converted to absolute CBF units based on the parameters above.

Evoked percent $CMRO_2$ changes during the visual and modified Stroop tasks were determined using the GCM as in Gauthier and Hoge (in press-a) and the M values estimated using the procedure described above over each task-specific ROI (Gauthier and Hoge, in press-b).

Other than the coordinates for intersection of group average M vs. OEF_0 curves, for which the range of intersection coordinates was used, all uncertainties are provided as ± standard error. Uncertainties on evoked $CMRO_2$ were computed from uncertainties on M, CBF and BOLD as described in Davis et al. (1998).

Visual ROI

Because responses to the flashing checkerboard are large enough to be detectable at the single subject level, regions of interest (ROIs) were derived from the intersection of the flow and BOLD thresholded ($p \leq 0.01$ corrected) (Worsley et al., 2002) visual activation T-maps for each individual subject from the NeuroLens analysis. One subject (subject 1) fell asleep during the visual task and was therefore excluded from all analyses requiring a visual ROI. The ROIs for the visual task are the same as presented in a previous report (Gauthier and Hoge, in press-a). The M parameter and evoked $CMRO_2$ data were

included in that publication and are reproduced here to facilitate comparison with the other ROIs. Baseline OEF_0 and $CMRO_2$ measures over this ROI represent however a novel result.

Stroop ROIs definition

Because the modified Stroop task yields smaller signal changes not readily detectable at the single subject level for a single run, individual subject ROIs for the Stroop task were defined from the significant BOLD signal changes during the inhibition/switching blocks for the seven participants included in this study. Two regions of interest were drawn for this task, one over bilateral frontal areas and one over parietal areas.

This analysis was done using FSL. All functional data were motion corrected with MCFLIRT (Jenkinson et al., 2002) and the brain was extracted using BET (Brain Extraction Tool, version 2.1) (Smith, 2002). A 6 mm^3 FWHM 3D Gaussian smoothing kernel, high-pass filter (100 s cutoff) and pre-whitening (FILM) (Woolrich et al., 2001) were applied to the time series. Spatial normalization to standard space (MNI152 template) (Jenkinson et al., 2002; Jenkinson and Smith, 2001) was performed (12 degrees of freedom) on the 30 ms echo time series. The BOLD time series was extracted from the second echo time series (TE = 30 ms) by isolating the control images from the original time series. A GLM was performed with the main experimental paradigm convolved with a dual gamma function. Temporal derivatives were included in the model. Fixed effect group analysis was performed using FLAME1 (Beckmann et al., 2003; Woolrich, 2008; Woolrich et al., 2004) to generate group average statistical maps for the contrast representing the subtraction of the control blocks from the Stroop blocks (isolating the areas specifically involved in inhibition/switching). The group average map thresholded at Z = 2.3 for the 30 ms echo was used to derive the individual ROIs. The transformations for spatial normalization of the seven subjects were inverted to project the group ROIs into individual subject space (Fig. 1) to perform ROI quantifications in native space.

In order to account for the fact that our large EPI voxels inevitably contained a mixture of grey matter, white matter, and CSF, average BOLD and ASL responses were determined by computing weighted-averages within ROIs, with the weighting provided by the estimated grey matter volume fraction in each voxel. The grey matter volume fraction was determined using automatic tissue segmentation of anatomical images using the FAST module of FSL (Zhang et al., 2001). Grey matter probability maps generated by FAST were projected into native EPI space using linear interpolation. Binarized individual ROI maps (both visual and Stroop task-derived) were multiplied by grey matter probability. This approach assumes that the responses in white matter and CSF are negligible compared with the grey matter response, which is supported by our observations in these tissue compartments (data not shown).

Results

Gas manipulations

All gas manipulations led to the expected changes in end-tidal gas partial pressures (Table 1). Breathing of 100% O_2 led to an increase in ETO_2 of 425.83 ± 31.28 mm Hg during the hyperoxia block. A slight hypocapnia was induced by the manipulation with a decrease in $ETCO_2$ of 3.21 ± 0.37 mm Hg. Breathing the 7% CO_2 in air mixture led to an average increase $ETCO_2$ of 9.04 ± 1.31 mm Hg, with a concomitant increase in ETO_2 from hyperventilation during the CO_2 block of 14.22 ± 2.08 mm Hg. Both ETO_2 and $ETCO_2$ were successfully elevated during breathing of 7% CO_2 in 93% O_2, with an $ETCO_2$ increase of 7.41 ± 0.65 mm Hg and an ETO_2 increase of 304.26 ± 26.85 mm Hg. The $ETCO_2$ and ETO_2 values during each breathing manipulations are given in Table 1.

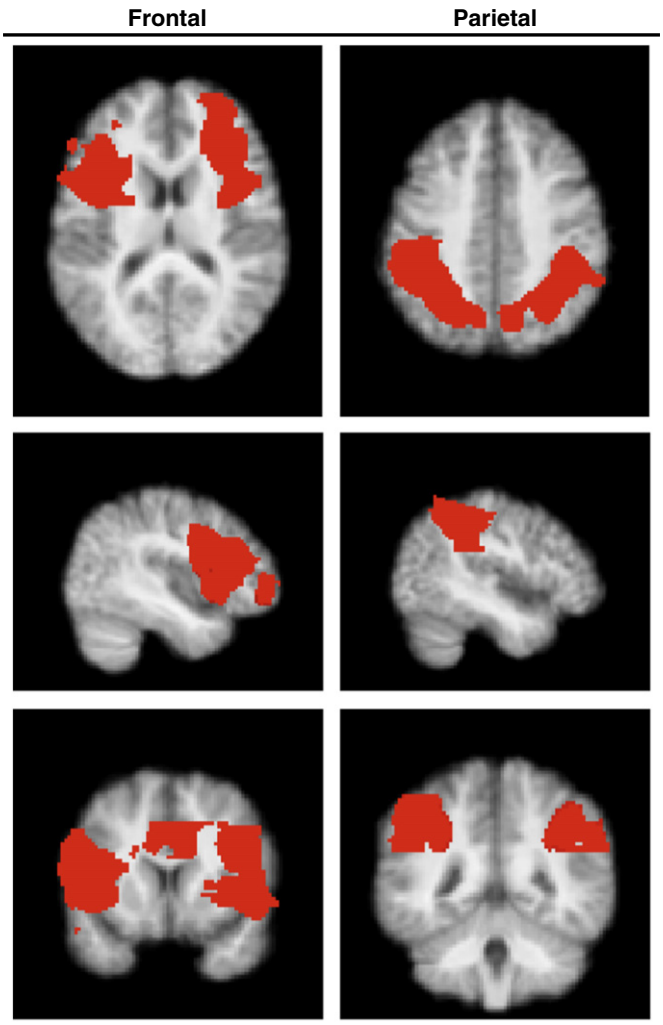

Fig. 1. ROI for Stroop task.ROIs for the modified Stroop task determined using the significant (Z ≥ 2.3) signal increases in BOLD group maps. Two regions were drawn to reflect the bilateral frontal and parietal components to the task.

The percent BOLD and CBF changes evoked by the three breathing manipulations are shown in Fig. 2. Percent CBF changes (Fig. 2A) are shown only for the hypercapnia (HC) and combined hyperoxia/hypercapnia (HO-HC) manipulations, since a fixed flow decrease was assumed for hyperoxia (see Methods). Similar average percent CBF changes were obtained for HC and HO-HC over all ROIs. Percent BOLD signal changes (Fig. 2B) are shown in response to all breathing manipulations. In general, as shown before (Gauthier and Hoge, in press-a,b), the amplitude of percent BOLD changes in response to hyperoxia and hypercapnia are approximately half of that found for combined hyperoxia/hypercapnia. Both percent CBF and BOLD changes show a trend towards lower amplitude signals in more frontal areas.

Table 1
Respiratory parameters. End-tidal CO_2 and O_2 values (mm Hg) for each breathing manipulations (hypercapnia, hyperoxia and combined hyperoxia/hypercapnia). These values are used in the GCM as a surrogate for arterial concentrations of gases.

	Hyperoxia	Hypercapnia	Combined
Baseline $ETCO_2$	40.11 ± 0.95	40.21 ± 0.68	40.63 ± 0.61
Manipulated $ETCO_2$	36.90 ± 0.88	49.26 ± 0.94	48.04 ± 0.82
Baseline ETO_2	117.54 ± 5.49	121.63 ± 6.68	116.92 ± 5.08
Manipulated ETO_2	543.37 ± 30.00	135.84 ± 5.29	421.18 ± 23.44

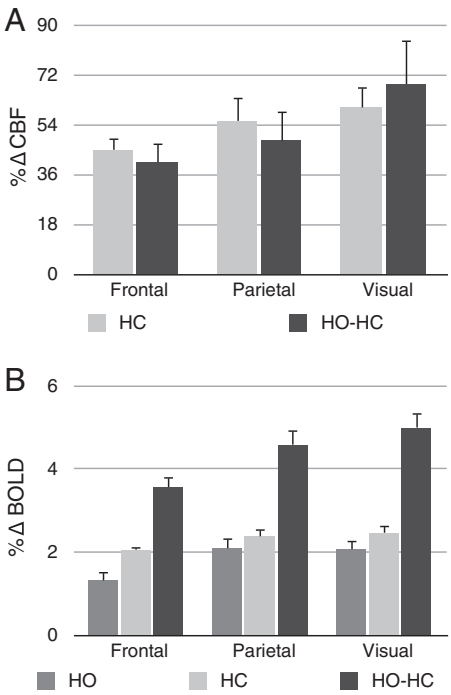

Fig. 2. Percent CBF and BOLD changes during breathing manipulations.Percent CBF (A) and BOLD (B) changes in response to hyperoxia (HO), hypercapnia (HC) and combined hyperoxia/hypercapnia (HO–HC) over the different functionally-determined ROIs. CBF changes to the hyperoxia manipulation are not given as they are too small to be measured reliably in small ROIs. Error bars represent the inter-subject standard error.

M, OEF_0 and resting $CMRO_2$

Percent changes in BOLD and CBF, as well as end-tidal PO_2 values at baseline and during the breathing manipulations were input into the GCM to construct the M vs. OEF_0 curves and solve for a unique value of M and OEF_0. Fig. 3 shows the graphs for each ROI, with a star representing the value used in subsequent analyses. The value for grey matter was taken from a previous study for visual comparison (Gauthier and Hoge, in press-b). It can be seen from these graphs that, while the three lines intersect at a common point for grey matter, they form a small triangle of intersection points around physiological values for the functionally-determined ROIs. The resulting M, OEF_0 and $CMRO_2$ estimates over the functional ROIs are shown in Fig. 4 and Table 2. M values were found to be similar over all areas, with values of $6.09 \pm 1.11\%$, $6.11 \pm 1.20\%$ and $5.94 \pm 1.08\%$ for the frontal, parietal and visual ROIs respectively. OEF_0 values were found to be close to literature values, with values of 0.45 ± 0.07, 0.29 ± 0.06 and 0.29 ± 0.05 for the frontal, parietal and visual ROIs respectively. Baseline $CMRO_2$ values of 173.62 ± 27.74 μmol/100 g/min, 99.59 ± 18.83 μmol/100 g/min and 125.09 ± 21.82 μmol/100 g/min were measured for the frontal, parietal and visual ROIs respectively.

Task-evoked $CMRO_2$

The M value used for evoked $CMRO_2$ calculations was taken as the average of the intersection point for the hypercapnia and hyperoxia curves and the intersection point for the combined hyperoxia/hypercapnia (carbogen) and the hyperoxia curves (represented by a star in each subplot within Fig. 3). Percent CBF (A) and BOLD (B) changes in response to the visual and Stroop tasks over their specific ROI (frontal and parietal ROIs for the Stroop task and the visual ROI for the flashing checkerboard stimulus) are shown in Fig. 5. CBF and BOLD percent changes in response to the visual task ($68.54 \pm 8.95\%$ and $1.31 \pm 0.11\%$ for CBF and BOLD respectively) were much larger than the percent changes in response to the modified Stroop task. The percent CBF changes during the Stroop task were $8.98 \pm 1.36\%$ and $14.47 \pm 1.84\%$ for frontal and parietal ROIs respectively. Percent BOLD signal changes during the Stroop task were $0.33 \pm 0.04\%$ and $0.43 \pm 0.07\%$ for frontal and parietal ROIs respectively. Percent $CMRO_2$ change evoked by the task were $3.87 \pm 1.20\%$ and $7.33 \pm 1.62\%$ over the frontal and parietal ROIs during performance of the modified Stroop task. The visual task evoked a larger $34.02 \pm 7.43\%$ increase in metabolism over the visual ROI. The percent increase in oxidative metabolism evoked by the tasks over the ROIs in units of μmol/100 g/min units are shown in Fig. 6.

Vascular and metabolic profile

Table 2 summarizes the vascular and metabolic information to be obtained from our technique. It includes the baseline absolute CBF in units of ml/100 g/min, cerebrovascular reactivity (CVR) in units of %Δ CBF/mm Hg, M in units of percent, OEF_0 and $CMRO_2$ at rest in units of μmol/100 g/min, percent evoked $CMRO_2$ during the two tasks and n, the value for flow-metabolic coupling. CVR corresponds to the increase in CBF per unit increase in $ETCO_2$ during the hypercapnia manipulation. The flow-metabolic coupling parameter n represents the percent flow increase during a task divided by the $CMRO_2$ increase during that same task.

Discussion

We have shown that our GCM framework allows absolute quantification of $CMRO_2$ and other physiological parameters both at rest and during task activation. In a previous report (Gauthier and Hoge, in press-b), we demonstrated the possibility of using the GCM with different combinations of hypercapnia and hyperoxia to estimate resting values of M and OEF_0 throughout grey matter. We have shown here that this approach can also be applied in the context of a task activation study. The M and OEF_0 values determined at rest can subsequently be combined with BOLD and CBF changes measured in response to a functional challenge, to yield task-evoked changes in $CMRO_2$ and flow-metabolism coupling. In all ROIs, a physiological value was estimated for the absolute resting CBF, cerebrovascular reactivity, the calibration factor M, OEF_0, $CMRO_2$ at rest, percent evoked $CMRO_2$ during both a visual and a modified Stroop task and n, the value for flow-metabolism coupling.

Accuracy of estimates

The values for M, OEF_0, baseline $CMRO_2$ and task-evoked $CMRO_2$ estimated using the method described here fall within the physiological range. While other MRI methods exist to obtain an estimate of these parameters (Bolar et al., 2011b; Bulte et al., 2011; Chiarelli et al., 2007; Davis et al., 1998; Fan et al., 2011; He and Yablonskiy, 2007; Jain et al., 2010; Xu et al., 2009), all methods rely on complex modeling and a certain number of assumptions. The M parameter is specific to MRI, since it represents the magnetic properties of baseline deoxyhemoglobin content, but nuclear medicine techniques can be used to assess oxidative metabolism. PET measurements of $CMRO_2$ and OEF rely on three separate acquisitions with injection of ^{15}O labeled O_2, H_2O and CO. These three measurements are necessary to model the combined contribution of O_2 diffusion into tissue, its conversion to water during oxidative metabolism, as well as the dependence on blood volume, assessed with $C^{15}O$ (Buxton, 2010; Mintun et al., 1984). While these PET measures of oxygen utilization are also indirect, and subject to their own sets of confounds, they can be used as a benchmark measure to assess qualitatively the accuracy of the estimates obtained using our technique.

Visual

Stimulation of primary visual cortex is commonly used to test new imaging techniques as it yields very large and reliably detectable signal

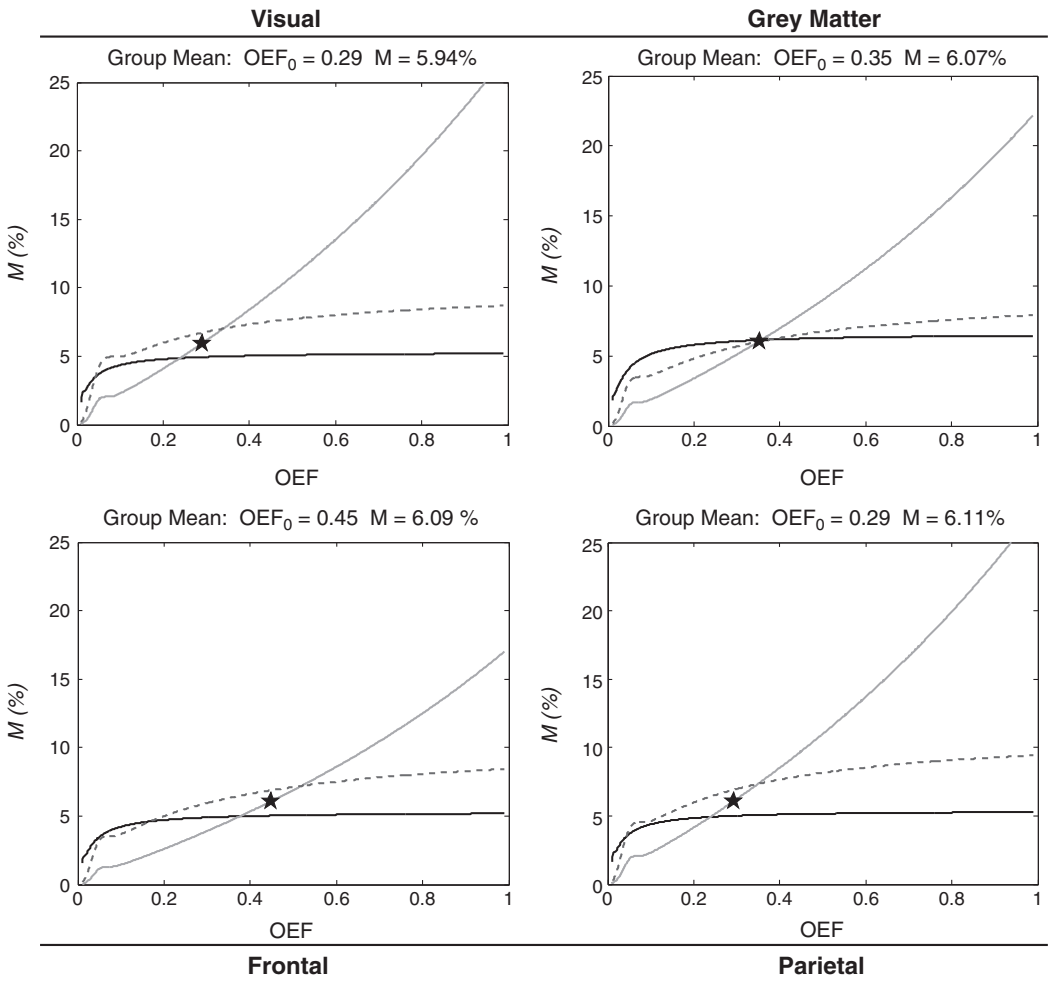

Fig. 3. Intersection plots for all ROIs.Plots of the M vs. OEF_0 curves estimated using the three gas manipulations over all ROIs. The star represents the solution for M and OEF_0. Solid grey lines show the curve for hyperoxia, solid black lines for hypercapnia and dashed black lines for combined hyperoxia/hypercapnia. The plot for grey matter (GM) group average values for the same group is taken from another study and included for comparison.

changes. The M value detected here for visual cortex of 5.94 ± 1.08 was at the lower end of the range of values found in literature. In a previous survey of 3T M values in visual cortex (in which M values were adjusted to reflect values at a TE of 30 ms) (Gauthier and Hoge, in press-a), we found values ranging from 5.3 (Bulte et al., 2009) to 12.1 (Perthen et al., 2008). Our own values, derived from simultaneous hypercapnia and hyperoxia manipulations (carbogen breathing) have in the past been typically slightly higher (Gauthier and Hoge, in press-a,b; Gauthier et al., 2011). This may however reflect the contribution in this case from all three gas manipulations in the determination of M and OEF_0, since hypercapnia and hyperoxia are associated with lower estimates for these parameters (Fig. 3) (Gauthier and Hoge, in press-a). Also, it is possible that the current estimate is a more accurate representation of grey matter values. The ROIs presented here include a reduced contribution from veins and other tissue types since we have corrected for grey matter probability when averaging over the ROIs.

The robust CBF and BOLD signal changes evoked by a flashing checkerboard led to a $34.02 \pm 7.43\%$ increase in oxidative metabolism from the value of 125.09 ± 21.82 μmol/100 g/min determined at rest. The values for percent evoked metabolism and flow metabolism coupling ratio ($n = 2.01 \pm 0.78$) found here were both consistent with previous reports using similar visual stimuli at 3T (Ances et al., 2008; Ances et al., 2009; Leontiev et al., 2007; Lin et al., 2008). The value for visual resting $CMRO_2$ determined here (125.09 ± 21.82 μmol/100 g/min) is somewhat lower than values obtained using ^{15}O-PET techniques in visual cortex, with values ranging from 169.2 ± 31.5 μmol/100 g/min to 206.5 ± 22.8 μmol/100 g/min (Ibaraki et al., 2008; Ishii et al., 1996; Mintun et al., 2002; Yamauchi et al., 2002). However, this may be due to the fact that the techniques use very different approaches to estimate metabolism, with different biases. Furthermore, since visual information is still present at rest, the value for baseline visual cortex metabolism must depend on the particular implementation of "rest". In this case, subjects had their eyes open, with gaze fixed on a white dot in the center of a uniform grey screen, with lights turned off in the scanner bore.

Literature MRI estimates of baseline OEF and $CMRO_2$ are not available for the visual cortex, but the value we observe for occipital cortex is well within the range observed for grey matter or whole brain, with values of 132 ± 20 μmol/100 g/min (Xu et al., 2009), 125 ± 15 μmol/100 g/min (Bolar et al., 2011a), 127 ± 6 (Jain et al., 2010), 151 ± 15 μmol/100 g/min (Fan et al., 2011) and 155 ± 39 μmol/100 g/min (Bulte et al., 2011) for MRI-derived estimates. This is also true of PET-derived grey-matter values, as indicated by a survey of literature PET values in Xu et al. (2009) showing values in young subjects spanning the range from 110.2 ± 19.6 μmol/100 g/min to 149.5 ± 27.5 μmol/100 g/min (Coles et al., 2006; Hattori et al., 2004; Ibaraki et al., 2008, 2010; Ishii et al., 1996; Ito et al., 2004, 2005). The conversion from ml/100 g/min to μmol/100 g/min was done using Eq. 5 from Gauthier et al. (Gauthier and Hoge, in press-b) starting with the values in the original papers rather than the values reported by Xu et al., which explains the slight discrepancies in the reported values.

Our OEF_0 estimate over visual cortex of 0.29 ± 0.05 is within the physiological range. Though this value is somewhat lower than values

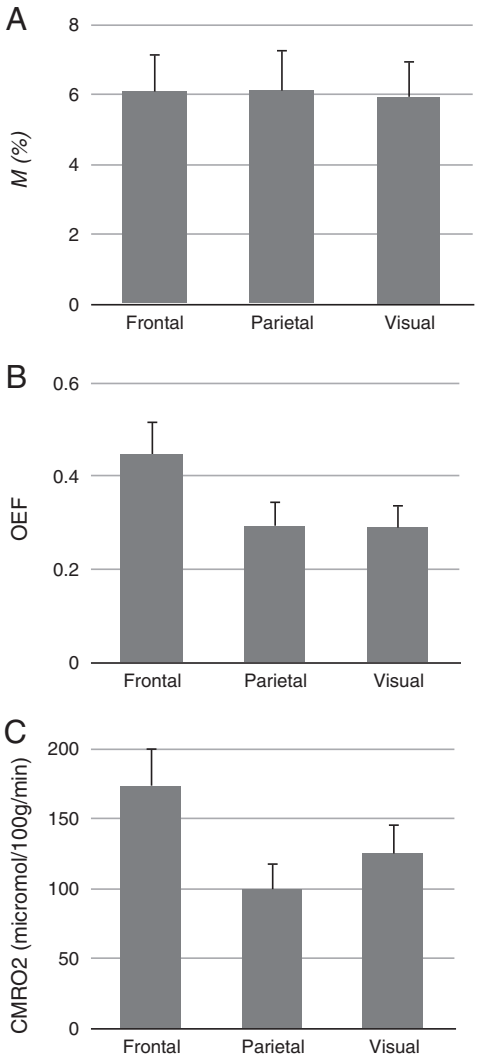

Fig. 4. M, OEF_0 and resting $CMRO_2$ values over all ROIs.Graphs of the M (A), OEF_0 (B) and resting $CMRO_2$ (C) values obtained over all ROIs. Error bars show the range of values used and represent the intersection point of the hypercapnia and hyperoxia curves and the intersection point of the combined hyperoxia/hypercapnia (carbogen) and hyperoxia curves.

reported in the PET literature, going from 0.36 ± 0.03 to 0.59 ± 0.06 (Ibaraki et al., 2008; Ito et al., 2005; Mintun et al., 2002; Yamauchi et al., 2002), it is similar to the value for grey matter (0.26 ± 0.02) and whole

Table 2
Vascular and metabolic profile. Values obtained from the different elements of our procedure to provide an overview of the vascular and metabolic properties of the different ROIs. It includes the baseline absolute CBF in units of ml/100 g/min, cerebrovascular reactivity (CVR) in units of %Δ CBF/mm Hg, M in units of percent, OEF_0 and $CMRO_2$ at rest in units of μmol/100 g/min, percent evoked $CMRO_2$ during the two tasks and n, the value for flow-metabolic coupling. CVR corresponds to the increase in CBF per unit increase in $ETCO_2$ during the hypercapnia manipulation. n represents the percent flow increase during a task divided by the $CMRO_2$ increase during that same task.

	Frontal	Parietal	Visual
Baseline CBF (ml/100 g/min)	48.88 ± 0.92	42.75 ± 3.00	54.45 ± 3.10
CVR (%ΔCBF/mm Hg)	5.44 ± 0.70	6.57 ± 0.94	7.48 ± 0.53
M (%)	6.09 ± 1.11	6.11 ± 1.20	5.94 ± 1.08
OEF_0	0.45 ± 0.07	0.29 ± 0.06	0.29 ± 0.05
$CMRO_2$ (μmol/100 g/min)	173.62 ± 27.74	99.59 ± 18.83	125.09 ± 21.82
%Δ $CMRO_2$	3.87 ± 1.20	7.33 ± 1.62	34.02 ± 7.43
n	3.32 ± 1.18	1.98 ± 0.80	2.01 ± 0.78

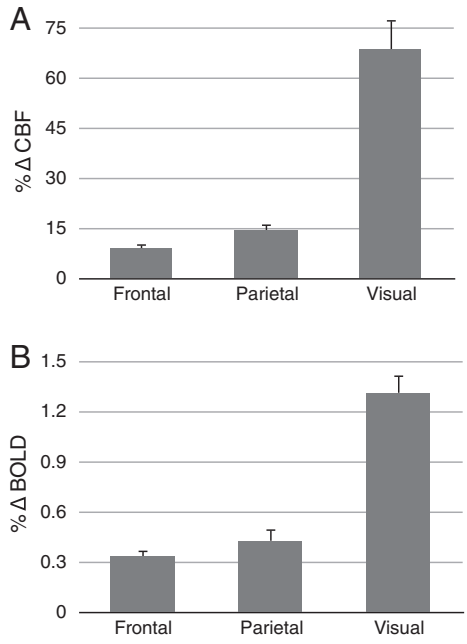

Fig. 5. Task-evoked percent CBF and BOLD changes.Average percent CBF (A) and BOLD (B) changes evoked by the modified Stroop (in Frontal and Parietal ROIs) and the visual (Visual) tasks. Error bars represent the inter-subject standard error.

brain (0.36 ± 0.02 and 0.38 ± 0.14) found using three other MRI techniques (Bolar et al., 2011a; Bulte et al., 2011). PET values over all grey matter from the literature range from 0.36 ± 0.06 to 0.44 ± 0.06. The fact that these are systematically higher than all MR-based estimated may indicate that the assumptions or noise biases for these two modalities pull estimates in opposite directions (Ibaraki et al., 2008; Ito et al., 2004; Yamaguchi et al., 1986). Further exploration is clearly warranted to assess the accuracy of these values.

Stroop

Cognitive tasks give rise to much more subtle signal changes than primary sensory stimuli and are generally used to assess neurological correlates of specific cognitive subcomponents. To reproduce this situation with the modified Stroop task used here, blocks of a more complex version of the task, that included components of inhibition and switching, were interspersed with blocks of a simpler version of the task that only required color-naming (no inhibition or switching). Though the signal changes to each version of the task were readily detectable, the difference between them was not. This is most likely due to both the small number of subjects included in this proof-of-concept study, but also to the fact that a single acquisition with the modified Stroop task was obtained for each subject. Because of this, we elected to use only the signal changes obtained during the

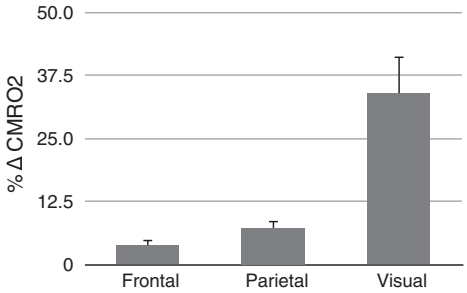

Fig. 6. Task-evoked percent $CMRO_2$ change.Percent task-evoked $CMRO_2$ change for the modified Stroop (in Frontal and Parietal ROIs) and the visual (Visual) tasks. Error bars represent the standard error obtained using the error analysis presented by Davis et al. (Davis et al., 1998).

inhibition/switching blocks, without subtracting from them the signal changes obtained in the control, simpler version of the task. It is to be noted that the lack of a significant difference in the fMRI signal changes obtained during the inhibition/switching and control blocks in the small cohort of subjects presented here is not due to an absence of behavioral effect of the task. This is indicated by the fact that participants performed significantly better both in terms of reaction time ($p = 0.003$) and accuracy ($p = 0.004$) during the control blocks as compared to the inhibition/switching blocks.

Testing the accuracy of values associated with the modified Stroop task is made more difficult by the fact that there are many versions of this task. The extent and exact localization of the significant signal changes will depend on the exact implementation of the task, but also on the SNR of the imaging technique used to detect the changes. Lower SNR techniques, such as ASL, may not be as efficient for the detection of small signal changes, especially in areas known to be more affected by distortions and signal losses due to susceptibility effects. Even with these potential confounds, the modified Stroop task has the advantage of having been extensively characterized using a variety of imaging techniques and some robust and conserved signal changes exist across modalities. Two main positive signal change foci were found here: an extensive bilateral frontal component covering parts of Brodmann areas 6, 9, 45 and 46, with partial extension into cingulate cortex around Brodmann area 32 and into part of the frontal pole. The second focus encompassed regions in parietal areas, covering mainly parts of bilateral Brodmann areas 7, 39 and 40. The frontal component corresponds well to the literature on the localization of activation during the inhibition component of Stroop and during task switching (Brass and von Cramon, 2002; Derrfuss et al., 2005; Leung et al., 2000; MacDonald et al., 2000; Milham et al., 2002; Zysset et al., 2007), while parietal activation has been observed during task switching (Brass and von Cramon, 2002; Dove et al., 2000; Kimberg et al., 2000; MacDonald et al., 2000; Yeung et al., 2006). A contribution from anterior cingulate cortex (Brodmann 32) was also detected, as expected in this type of task (Brass and von Cramon, 2002; Derrfuss et al., 2005; Leung et al., 2000; MacDonald et al., 2000; Milham et al., 2002; Zysset et al., 2007). We also detected a frontal pole component, thought to reflect the flexibility required to inhibit automatic responses in the context of changing stimulus contingencies (Nobre et al., 1999).

Only three calibrated fMRI studies have so far looked at cognitive tasks (Goodwin et al., 2009; Mohtasib et al., 2012; Restom et al., 2008), two of them using the Stroop task with the hyperoxia calibration method (Goodwin et al., 2009; Mohtasib et al., 2012). In Goodwin et al. (2009), M values were found to be higher than in the present study both in frontal (9.0 ± 5.8 and 7.4 ± 4.0 for left and right middle frontal gyri respectively) and parietal (10.2 ± 4.9 and 7.7 ± 4.4 for left and right parietal lobules respectively) regions, though the value found here is within the standard deviation of that study. The M values obtained using the same task in a slightly larger cohort in Mohtasib et al. (2012) of 5.6 ± 0.7 and 6.0 ± 0.6 for left and right middle frontal gyri respectively agrees closely with the value of 6.09 ± 1.11 found here for bilateral frontal areas. Values for the flow-metabolism coupling parameter n in medial frontal areas in Mohtasib et al. (2012) were in good agreement with the value for frontal areas found here. Literature flow metabolism coupling values are not available for the regions corresponding to our other ROIs, but these fall within the physiological expected range with values close to two (Table 2).

OEF_0 values for medial frontal areas fell within the expected range with a value of 0.45 ± 0.07. This estimate is consistent with the literature estimates in frontal areas of 0.41 ± 0.07 and 0.35 ± 0.06 (Ibaraki et al., 2008; Ishii et al., 1996). Our parietal estimate was however below literature estimates with a value of 0.29 ± 0.06 as compared to the literature values of 0.41 ± 0.07 and 0.40 ± 0.05 for that region (Ibaraki et al., 2008; Ishii et al., 1996). The accuracy of $CMRO_2$ estimates shows a similar pattern as OEF values. Our frontal values of 173.62 $\pm$ 27.74 μmol/100 g/min for the frontal ROI is somewhat higher than literature estimates of 133.8 ± 23.6 and 137.7 ± 25.2 μmol/100 g/min for frontal lobes (Ibaraki et al., 2008; Ishii et al., 1996). Our parietal estimate of 99.59 ± 18.83 μmol/100 g/min is however lower than literature values of 153.4 ± 31.4 and 141.6 ± 23.6 μmol/100 g/min (Ibaraki et al., 2008; Ishii et al., 1996). The discrepancy between the values presented here and the PET literature values may reflect the fact that more subjects are required for robust characterization of a cognitive task, since signal changes in the areas involved are more subtle.

A recent paper by Bulte et al. (2011) uses a technique similar to ours to measure the same set of physiological parameters. In brief, this study uses a hypercapnia manipulation to derive M using the Davis model (Davis et al., 1998), then uses this M value in the context of a hyperoxia manipulation to calculate OEF_0 using the Chiarelli model (Chiarelli et al., 2007). Conceptually very close to the method proposed here, we would expect the values obtained by both methods to be quite similar. Though the method proposed by Bulte and colleagues has so far only been applied to complete grey matter, the values agree very well with our own grey matter values published in a previous report (Gauthier and Hoge, in press-b). Though values are not available for smaller ROIs, the close agreement in the values obtained through both methods in different subjects is an encouraging sign that these techniques may provide valid estimates of baseline OEF and $CMRO_2$.

Implementation biases and confounds

All baseline measures were found to be in the physiological range, but somewhat different from PET-derived estimates. This could be due to inherent biases associated with each method and their underlying assumptions, especially since all methods include a substantial component of modeling. While we feel that the current results support the general validity of the GCM framework, the ultimate precision of the method will clearly benefit from further optimization. Moreover, the small number of subjects included in this proof-of-concept study highlights the increased challenge of quantifying cognitive responses compared with the much more robust responses to primary sensory stimulation. While the intersection plots obtained in grey matter are generally robust and adequate for quantification, data obtained in smaller ROIs show a reduced precision and robustness to errors in measurement. While visual estimates may be somewhat spared given the large signal changes obtained in visual cortical areas, it is clear that a much larger cohort would be required for robust characterization of cognitive effects.

The precision of this method in dependent on the coincidence of intersection points between the curves generated from the three breathing manipulations. Inspection of the three curve plots from Fig. 3 shows that since the three intersection points are not coincident in these ROIs, the value of the final estimate depends on the relative position of the curves. In all cases, the curve for the combined hyperoxia/hypercapnia (HO-HC) breathing manipulation intersects the O_2 manipulation (HO) curve at a higher point (for both M and OEF_0) than the hypercapnia manipulation (HC) curve. Since the estimate reported here corresponds to the average between these two intersection points, a systematic downward bias in the HC curve (or upward bias in the combined HO-HC curve) will result in a similar bias in the final estimate.

While we cannot rule out conclusively the possibility that this relationship between the curves is due to a systematic error introduced by our model, the fact that with enough averaging (as in the case of complete grey matter ROIs) we obtain tight convergence suggests that this divergence may instead be due to systematic bias arising from the lower SNR obtained with small ROIs. The model includes ratio estimates and non-linear terms, which are prone to bias under low SNR conditions. Since the quality of the ultimate measurements is mainly limited by the quality of the ASL data, and since accurate CBF

measurements of the changes associated with breathing manipulations are known to be difficult to obtain (Tancredi et al., 2012), it is possible that this systematic bias may arise from suboptimal measurement of flow changes during gas manipulations. To rule this out, future studies will use ASL methods yielding improved measurements of gas manipulations. Strategies to improve ASL quality could include using multiple delay times to capture the temporal profile of tag delivery at each voxel, which can then be fit with a kinetic model (Buxton et al., 1998) to provide a more accurate estimate of flow (Bulte et al., 2011). Another possibility would be to implement background suppression techniques to reduce the physiological or instrumental modulation of the background "static" tissue signal that is unrelated to flow (Dixon et al., 1991; Maleki et al., 2011).

Alternatively, this effect could arise from errors in the BOLD signal change measurement. The BOLD response to hypercapnia has a lower amplitude than the BOLD response to combined HO-HC. This smaller response means that the contrast-to-noise ratio (CNR) of the hypercapnia BOLD experiment is lower than that of combined HO-HC, given a similar level of noise in both measurements. This reduced CNR could lead to an underestimation of the BOLD response to hypercapnia, thereby leading to an underestimation of the M value associated with a given OEF. This underestimation would be reduced for combined HO-HC, since the measured BOLD changes are larger and therefore easier to measure against a similar level of noise.

The values for all parameters were estimated over functionally-defined ROIs using fairly large voxels. It is likely therefore that the measurements suffer from biases due to some inclusion of cerebro-spinal fluid (CSF) and white matter through partial volume effects. ASL is a low SNR technique and large voxels are therefore necessary to obtain meaningful measurement values. For the same reason, good quality single voxel and small ROI estimates are difficult to obtain. However, by weighting each voxel within the ROI by the grey matter volume, estimated for that voxel using automatic tissue segmentation, this is unlikely to be the major factor at play to explain divergence of the curves.

The technique chosen to administer the gases, by delivering gases of fixed mixture concentrations through an unsealed face mask gives rise to somewhat variable end-tidal gas concentrations. While other techniques exist to more accurately control and target specific end-tidal values of CO_2 and O_2 (Mark et al., 2010; Slessarev et al., 2007), fluctuations over a moderate range are of no significant consequence for the method described here, as long as end-tidal measurements are performed. The variability in end-tidal values could furthermore be reduced by using a mask with a larger inflow bag and a regulator allowing higher flow rates. This would allow the mask to be sealed to the face and prevent room air from being entrained into the mask during periods of hyperventilation. Also, the use of a metronome to control breathing rate could help reduce inter-subject and inter-run variability. Finally, inhalation of CO_2 may be uncomfortable in high concentrations and lead to important changes in breathing pattern and attentional state that could potentially affect the results obtained using this approach. In this case however, subjects in general found the inhalation of 7% CO_2 to be quite tolerable with this specific setup, as indicated by the range of responses given on our subjective rating questionnaire. Average rating was 2.1 ± 0.6 over all subject, indicating a very low level of breathing discomfort.

One of the most debated assumptions of calibrated fMRI is that gas manipulations do not affect oxidative metabolism. Short periods of hyperoxia are not usually assumed to change metabolism, though some groups report a suppressive effect of O_2 on oxidative metabolism (Xu et al., 2011a). Furthermore, there is no consensus about the effects of hypercapnia with some studies reporting increases in metabolism (Horvath et al., 1994; Jones et al., 2005), decreases (Xu et al., 2011b; Zappe et al., 2008), and no detectable change (Chen and Pike, 2010a; Hino et al., 2000; McPherson et al., 1991). In a previous report (Gauthier and Hoge, in press-b), we have modeled the effects of both decreased and increased $CMRO_2$ on our model. Modeling the effects of decreases or increases in $CMRO_2$ during hypercapnia manipulations resulted in reduced convergence towards a unique solution for the intersection of the HC, HO and combined HO-HC curves. Because this intersection point corresponds to a baseline physiological property of the brain, a single point is expected. While the latter observations were not compatible with a significant CO_2-induced change in $CMRO_2$, results of other studies (Xu et al., 2011b; Zappe et al., 2008) have suggested there may be such an effect. It is clear that further exploration of the impact of CO_2 on $CMRO_2$ in different brain systems and under different conditions is required.

The selection of values for model parameters α and β has also been the subject of some contention. We used here values of $\alpha = 0.18$ and $\beta = 1.5$. This value for α is taken from experimental measurements of venous blood volume change (Chen and Pike, 2009, 2010b). Though β was originally taken to reflect the field-specific effects of deoxyhemoglobin on R_2^*, it can instead be viewed as a lumped constant encompassing additional physiological and physical factors. Numerical simulations published by Griffeth et al. suggested that, in an application of the original Davis model, consistency with an alternate multi-compartment model was maximized using a value of $\beta = 0.91$ (Griffeth and Buxton, 2011). Although we have chosen to adhere to the original definitions and currently "standard" values of α and β for the present study, alternate values such as those proposed by Griffeth could readily be inserted in the method presented here.

Conclusion

We have demonstrated that QUO2 MRI allows absolute quantification of $CMRO_2$ both at rest and in the context of a functional challenge. Additional quantitative information on resting physiology is also furnished, including resting CBF, CVR, M and OEF_0. The sensitivity of the method is limited mainly by the low SNR inherent in currently available ASL techniques, so while reliable quantification was achieved for visual stimulation, a substantially larger cohort would be required for precise characterization of a cognitive process like the inhibition and switching components of the modified Stroop task. The lower SNR conditions prevailing in the functionally defined ROIs highlight the possibility of systematic error related either to noise bias or regional differences that are not captured in the model, motivating further experimental and theoretical exploration. Significant improvements in ASL performance will be required for application of this method in individual patients or subjects.

Acknowledgments

We thank Carollyn Hurst, André Cyr and Tarik Hafyane for their help with data acquisition, Felipe Tancredi and Maude Laguë-Bauvais for the helpful discussions. We would also like to thank Jiongjiong Wang, who provided the pseudo-continuous arterial spin-labeling sequence used. This work was supported by the Canadian Institutes for Health Research (MOP 84378, Banting and Best Scholarship held by CJG), the Canadian Foundation for Innovation (Leaders Opportunity Fund 17380), and the Ministère du développement économique, de l'innovation et de l'exportation (PSR-SIIRI-239).

References

Ances, B.M., Leontiev, O., Perthen, J.E., Liang, C., Lansing, A.E., Buxton, R.B., 2008. Regional differences in the coupling of cerebral blood flow and oxygen metabolism changes in response to activation: implications for BOLD-fMRI. Neuroimage 39, 1510–1521.

Ances, B.M., Liang, C.L., Leontiev, O., Perthen, J.E., Fleisher, A.S., Lansing, A.E., Buxton, R.B., 2009. Effects of aging on cerebral blood flow, oxygen metabolism, and blood oxygenation level dependent responses to visual stimulation. Hum Brain Mapp 30, 1120–1132.

Banzett, R.B., Lansing, R.W., Evans, K.C., Shea, S.A., 1996. Stimulus–response characteristics of CO_2-induced air hunger in normal subjects. Respir Physiol 103, 19–31.

Beckmann, C.F., Jenkinson, M., Smith, S.M., 2003. General multilevel linear modeling for group analysis in FMRI. Neuroimage 20, 1052–1063.
Bohnen, N., Jolles, J., Twijnstra, A., 1992. Modification of the Stroop Color Word Test improves differentiation between patients with mild head injury and matched controls. Clinical Neuropsychologist 6, 178–184.
Bolar, D.S., Rosen, B.R., Sorensen, A.G., Adalsteinsson, E., 2011a. QUantitative Imaging of eXtraction of oxygen and TIssue consumption (QUIXOTIC) using venular-targeted velocity-selective spin labeling. Magn Reson Med 66 (6), 1550–1562.
Bolar, D.S., Rosen, B.R., Sorensen, A.G., Adalsteinsson, E., 2011b. QUantitative Imaging of eXtraction of oxygen and TIssue consumption (QUIXOTIC) using venular-targeted velocity-selective spin labeling. Magn Reson Med.
Brass, M., von Cramon, D.Y., 2002. The role of the frontal cortex in task preparation. Cereb Cortex 12, 908–914.
Bulte, D.P., Chiarelli, P.A., Wise, R.G., Jezzard, P., 2007. Cerebral perfusion response to hyperoxia. J Cereb Blood Flow Metab 27, 69–75.
Bulte, D.P., Drescher, K., Jezzard, P., 2009. Comparison of hypercapnia-based calibration techniques for measurement of cerebral oxygen metabolism with MRI. Magn Reson Med 61, 391–398.
Bulte, D.P., Kelly, M., Germuska, M., Xie, J., Chappell, M.A., Okell, T.W., Bright, M.G., Jezzard, P., 2011. Quantitative measurement of cerebral physiology using respiratory-calibrated MRI. Neuroimage 60 (1), 582–591.
Buxton, R.B., 2010. Interpreting oxygenation-based neuroimaging signals: the importance and the challenge of understanding brain oxygen metabolism. Front Neuroenergetics 2, 8.
Buxton, R.B., Frank, L.R., Wong, E.C., Siewert, B., Warach, S., Edelman, R.R., 1998. A general kinetic model for quantitative perfusion imaging with arterial spin labeling. Magn Reson Med 40, 383–396.
Chalela, J.A., Alsop, D.C., Gonzalez-Atavales, J.B., Maldjian, J.A., Kasner, S.E., Detre, J.A., 2000. Magnetic resonance perfusion imaging in acute ischemic stroke using continuous arterial spin labeling. Stroke 31, 680–687.
Chen, J.J., Pike, G.B., 2009. BOLD-specific cerebral blood volume and blood flow changes during neuronal activation in humans. NMR Biomed 22, 1054–1062.
Chen, J.J., Pike, G.B., 2010a. Global cerebral oxidative metabolism during hypercapnia and hypocapnia in humans: implications for BOLD fMRI. J Cereb Blood Flow Metab 30, 1094–1099.
Chen, J.J., Pike, G.B., 2010b. MRI measurement of the BOLD-specific flow-volume relationship during hypercapnia and hypocapnia in humans. Neuroimage 53, 383–391.
Chiarelli, P.A., Bulte, D.P., Wise, R., Gallichan, D., Jezzard, P., 2007. A calibration method for quantitative BOLD fMRI based on hyperoxia. Neuroimage 37, 808–820.
Coles, J.P., Fryer, T.D., Bradley, P.G., Nortje, J., Smielewski, P., Rice, K., Clark, J.C., Pickard, J.D., Menon, D.K., 2006. Intersubject variability and reproducibility of 15O PET studies. J Cereb Blood Flow Metab 26, 48–57.
Cox, R.W., Jesmanowicz, A., 1999. Real-time 3D image registration for functional MRI. Magn Reson Med 42, 1014–1018.
Davis, T.L., Kwong, K.K., Weisskoff, R.M., Rosen, B.R., 1998. Calibrated functional MRI: mapping the dynamics of oxidative metabolism. Proc Natl Acad Sci U S A 95, 1834–1839.
Derrfuss, J., Brass, M., Neumann, J., von Cramon, D.Y., 2005. Involvement of the inferior frontal junction in cognitive control: meta-analyses of switching and Stroop studies. Hum Brain Mapp 25, 22–34.
Dixon, W.T., Sardashti, M., Castillo, M., Stomp, G.P., 1991. Multiple inversion recovery reduces static tissue signal in angiograms. Magn Reson Med 18, 257–268.
Dove, A., Pollmann, S., Schubert, T., Wiggins, C.J., von Cramon, D.Y., 2000. Prefrontal cortex activation in task switching: an event-related fMRI study. Brain Res Cogn Brain Res 9, 103–109.
Fan, A.P., Benner, T., Bolar, D.S., Rosen, B.R., Adalsteinsson, E., 2011. Phase-based regional oxygen metabolism (PROM) using MRI. Magn Reson Med. 67 (3), 669–678.
Gauthier, C.J., Hoge, R.D., in press-a. A generalized procedure for calibrated MRI incorporating hyperoxia and hypercapnia. Hum. Brain Mapp.
Gauthier, C.J., Hoge, R.D., in press-b. Magnetic resonance imaging of resting OEF and CMRO2 using a generalized calibration model for hypercapnia and hyperoxia. Neuroimage. 60(2):1212-25.
Gauthier, C.J., Madjar, C., Tancredi, F.B., Stefanovic, B., Hoge, R.D., 2011. Elimination of visually evoked BOLD responses during carbogen inhalation: implications for calibrated MRI. Neuroimage 54, 1001–1011.
Glover, G.H., 1999. Deconvolution of impulse response in event-related BOLD fMRI. Neuroimage 9, 416–429.
Goodwin, J.A., Vidyasagar, R., Balanos, G.M., Bulte, D., Parkes, L.M., 2009. Quantitative fMRI using hyperoxia calibration: reproducibility during a cognitive Stroop task. Neuroimage 47, 573–580.
Griffeth, V.E., Buxton, R.B., 2011. A theoretical framework for estimating cerebral oxygen metabolism changes using the calibrated-BOLD method: modeling the effects of blood volume distribution, hematocrit, oxygen extraction fraction, and tissue signal properties on the BOLD signal. Neuroimage 58, 198–212.
Griswold, M.A., Jakob, P.M., Heidemann, R.M., Nittka, M., Jellus, V., Wang, J., Kiefer, B., Haase, A., 2002. Generalized autocalibrating partially parallel acquisitions (GRAPPA). Magn Reson Med 47, 1202–1210.
Hattori, N., Bergsneider, M., Wu, H.M., Glenn, T.C., Vespa, P.M., Hovda, D.A., Phelps, M.E., Huang, S.C., 2004. Accuracy of a method using short inhalation of (15)O-O(2) for measuring cerebral oxygen extraction fraction with PET in healthy humans. J Nucl Med 45, 765–770.
He, X., Yablonskiy, D.A., 2007. Quantitative BOLD: mapping of human cerebral deoxygenated blood volume and oxygen extraction fraction: default state. Magn Reson Med 57, 115–126.
He, X., Zhu, M., Yablonskiy, D.A., 2008. Validation of oxygen extraction fraction measurement by qBOLD technique. Magn Reson Med 60, 882–888.
Hino, J.K., Short, B.L., Rais-Bahrami, K., Seale, W.R., 2000. Cerebral blood flow and metabolism during and after prolonged hypercapnia in newborn lambs. Crit Care Med 28, 3505–3510.
Hoge, R.D., Atkinson, J., Gill, B., Crelier, G.R., Marrett, S., Pike, G.B., 1999. Investigation of BOLD signal dependence on cerebral blood flow and oxygen consumption: the deoxyhemoglobin dilution model. Magn Reson Med 42, 849–863.
Horvath, I., Sandor, N.T., Ruttner, Z., McLaughlin, A.C., 1994. Role of nitric oxide in regulating cerebrocortical oxygen consumption and blood flow during hypercapnia. J Cereb Blood Flow Metab 14, 503–509.
Ibaraki, M., Miura, S., Shimosegawa, E., Sugawara, S., Mizuta, T., Ishikawa, A., Amano, M., 2008. Quantification of cerebral blood flow and oxygen metabolism with 3-dimensional PET and 15O: validation by comparison with 2-dimensional PET. J Nucl Med 49, 50–59.
Ibaraki, M., Shinohara, Y., Nakamura, K., Miura, S., Kinoshita, F., Kinoshita, T., 2010. Interindividual variations of cerebral blood flow, oxygen delivery, and metabolism in relation to hemoglobin concentration measured by positron emission tomography in humans. J Cereb Blood Flow Metab 30, 1296–1305.
Ishii, K., Sasaki, M., Kitagaki, H., Sakamoto, S., Yamaji, S., Maeda, K., 1996. Regional difference in cerebral blood flow and oxidative metabolism in human cortex. J Nucl Med 37, 1086–1088.
Ito, H., Kanno, I., Kato, C., Sasaki, T., Ishii, K., Ouchi, Y., Iida, A., Okazawa, H., Hayashida, K., Tsuyuguchi, N., Kuwabara, Y., Senda, M., 2004. Database of normal human cerebral blood flow, cerebral blood volume, cerebral oxygen extraction fraction and cerebral metabolic rate of oxygen measured by positron emission tomography with 15O-labelled carbon dioxide or water, carbon monoxide and oxygen: a multicentre study in Japan. Eur J Nucl Med Mol Imaging 31, 635–643.
Ito, H., Ibaraki, M., Kanno, I., Fukuda, H., Miura, S., 2005. Changes in cerebral blood flow and cerebral oxygen metabolism during neural activation measured by positron emission tomography: comparison with blood oxygenation level-dependent contrast measured by functional magnetic resonance imaging. J Cereb Blood Flow Metab 25, 371–377.
Jain, V., Langham, M.C., Wehrli, F.W., 2010. MRI estimation of global brain oxygen consumption rate. J Cereb Blood Flow Metab 30, 1598–1607.
Jenkinson, M., Smith, S., 2001. A global optimisation method for robust affine registration of brain images. Med Image Anal 5, 143–156.
Jenkinson, M., Bannister, P., Brady, M., Smith, S., 2002. Improved optimization for the robust and accurate linear registration and motion correction of brain images. Neuroimage 17, 825–841.
Jones, M., Berwick, J., Hewson-Stoate, N., Gias, C., Mayhew, J., 2005. The effect of hypercapnia on the neural and hemodynamic responses to somatosensory stimulation. Neuroimage 27, 609–623.
Kimberg, D.Y., Aguirre, G.K., D'Esposito, M., 2000. Modulation of task-related neural activity in task-switching: an fMRI study. Brain Res Cogn Brain Res 10, 189–196.
Leontiev, O., Dubowitz, D.J., Buxton, R.B., 2007. CBF/CMRO2 coupling measured with calibrated BOLD fMRI: sources of bias. Neuroimage 36, 1110–1122.
Leung, H.C., Skudlarski, P., Gatenby, J.C., Peterson, B.S., Gore, J.C., 2000. An event-related functional MRI study of the stroop color word interference task. Cereb Cortex 10, 552–560.
Lin, A.L., Fox, P.T., Yang, Y., Lu, H., Tan, L.H., Gao, J.H., 2008. Evaluation of MRI models in the measurement of CMRO2 and its relationship with CBF. Magn Reson Med 60, 380–389.
Liu, T.T., Wong, E.C., 2005. A signal processing model for arterial spin labeling functional MRI. Neuroimage 24, 207–215.
MacDonald III, A.W., Cohen, J.D., Stenger, V.A., Carter, C.S., 2000. Dissociating the role of the dorsolateral prefrontal and anterior cingulate cortex in cognitive control. Science 288, 1835–1838.
Maleki, N., Dai, W., Alsop, D.C., 2011. Optimization of background suppression for arterial spin labeling perfusion imaging. MAGMA 25 (2), 127–133.
Mark, C.I., Slessarev, M., Ito, S., Han, J., Fisher, J.A., Pike, G.B., 2010. Precise control of end-tidal carbon dioxide and oxygen improves BOLD and ASL cerebrovascular reactivity measures. Magn Reson Med. 64 (3), 749–756.
McPherson, R.W., Derrer, S.A., Traystman, R.J., 1991. Changes in cerebral CO_2 responsivity over time during isoflurane anesthesia in the dog. J Neurosurg Anesthesiol 3, 12–19.
Milham, M.P., Erickson, K.I., Banich, M.T., Kramer, A.F., Webb, A., Wszalek, T., Cohen, N.J., 2002. Attentional control in the aging brain: insights from an fMRI study of the stroop task. Brain Cogn 49, 277–296.
Mintun, M.A., Raichle, M.E., Martin, W.R., Herscovitch, P., 1984. Brain oxygen utilization measured with O-15 radiotracers and positron emission tomography. J Nucl Med 25, 177–187.
Mintun, M.A., Vlassenko, A.G., Shulman, G.L., Snyder, A.Z., 2002. Time-related increase of oxygen utilization in continuously activated human visual cortex. Neuroimage 16, 531–537.
Mohtasib, R.S., Lumley, G., Goodwin, J.A., Emsley, H.C., Sluming, V., Parkes, L.M., 2012. Calibrated fMRI during a cognitive Stroop task reveals reduced metabolic response with increasing age. Neuroimage 59, 1143–1151.
Nobre, A.C., Coull, J.T., Frith, C.D., Mesulam, M.M., 1999. Orbitofrontal cortex is activated during breaches of expectation in tasks of visual attention. Nat Neurosci 2, 11–12.
Perthen, J.E., Lansing, A.E., Liau, J., Liu, T.T., Buxton, R.B., 2008. Caffeine-induced uncoupling of cerebral blood flow and oxygen metabolism: a calibrated BOLD fMRI study. Neuroimage 40, 237–247.
Press, W.H., Flannery, B.P., Teukolsky, S.A., Vetterling, W.T., 1992. Numerical Recipes in C: The Art of Scientific Computing, 2nd ed. Cambridge University Press.
Restom, K., Perthen, J.E., Liu, T.T., 2008. Calibrated fMRI in the medial temporal lobe during a memory-encoding task. Neuroimage 40, 1495–1502.
Rhoades, R., Bell, D.R., 2009. Medical physiology: principles for clinical medicine, 3rd ed. Lippincott Williams & Wilkins, Philadelphia, Pa.; London.

Severinghaus, J.W., 1989. Water vapor calibration errors in some capnometers: respiratory conventions misunderstood by manufacturers? Anesthesiology 70, 996–998.
Slessarev, M., Han, J., Mardimae, A., Prisman, E., Preiss, D., Volgyesi, G., Ansel, C., Duffin, J., Fisher, J.A., 2007. Prospective targeting and control of end-tidal CO_2 and O_2 concentrations. J Physiol 581, 1207–1219.
Smith, S.M., 2002. Fast robust automated brain extraction. Hum Brain Mapp 17, 143–155.
Tancredi, F.B., Gauthier, C.J., Madjar, C., Bolar, D.S., Fisher, J.A., Wang, D.J., Hoge, R.D., 2012. Comparison of pulsed and pseudocontinuous arterial spin-labeling for measuring CO(2)-induced cerebrovascular reactivity. J Magn Reson Imaging 36 (2), 312–321.
Wang, J., Aguirre, G.K., Kimberg, D.Y., Roc, A.C., Li, L., Detre, J.A., 2003. Arterial spin labeling perfusion fMRI with very low task frequency. Magn Reson Med 49, 796–802.
Wasylyshyn, C., Verhaeghen, P., Sliwinski, M.J., 2011. Aging and task switching: a meta-analysis. Psychol Aging 26, 15–20.
Woolrich, M., 2008. Robust group analysis using outlier inference. Neuroimage 41, 286–301.
Woolrich, M.W., Ripley, B.D., Brady, M., Smith, S.M., 2001. Temporal autocorrelation in univariate linear modeling of FMRI data. Neuroimage 14, 1370–1386.
Woolrich, M.W., Behrens, T.E., Beckmann, C.F., Jenkinson, M., Smith, S.M., 2004. Multilevel linear modelling for FMRI group analysis using Bayesian inference. Neuroimage 21, 1732–1747.
Worsley, K.J., Liao, C.H., Aston, J., Petre, V., Duncan, G.H., Morales, F., Evans, A.C., 2002. A general statistical analysis for fMRI data. Neuroimage 15, 1–15.
Wu, W.C., Fernandez-Seara, M., Detre, J.A., Wehrli, F.W., Wang, J., 2007. A theoretical and experimental investigation of the tagging efficiency of pseudocontinuous arterial spin labeling. Magn Reson Med 58, 1020–1027.
Xu, F., Ge, Y., Lu, H., 2009. Noninvasive quantification of whole-brain cerebral metabolic rate of oxygen (CMRO2) by MRI. Magn Reson Med 62, 141–148.
Xu, F., Uh, J., Brier, M.R., Hart Jr., J., Yezhuvath, U.S., Gu, H., Yang, Y., Lu, H., 2011a. The influence of carbon dioxide on brain activity and metabolism in conscious humans. J Cereb Blood Flow Metab 31, 58–67.
Xu, F., Liu, P., Lu, H., 2011b. Effect of graded O_2 challenge on vascular and metabolic parameters. Proc. Intl. Soc. Mag. Reson. Med. 19th annual meeting, p. 765.
Yamaguchi, T., Kanno, I., Uemura, K., Shishido, F., Inugami, A., Ogawa, T., Murakami, M., Suzuki, K., 1986. Reduction in regional cerebral metabolic rate of oxygen during human aging. Stroke 17, 1220–1228.
Yamauchi, H., Okazawa, H., Kishibe, Y., Sugimoto, K., Takahashi, M., 2002. Changes in blood flow and oxygen metabolism during visual stimulation in carotid artery disease: effect of baseline perfusion and oxygen metabolism. Stroke 33, 1294–1300.
Yeung, N., Nystrom, L.E., Aronson, J.A., Cohen, J.D., 2006. Between-task competition and cognitive control in task switching. J Neurosci 26, 1429–1438.
Yun, J.Y., Lee, D.Y., Seo, E.H., Choo, I.H., Park, S.Y., Kim, S.G., Woo, J.I., 2011. Neural Correlates of Stroop Performance in Alzheimer's Disease: A FDG-PET Study. Dement Geriatr Cogn Dis Extra 1, 190–201.
Zaharchuk, G., Martin, A.J., Dillon, W.P., 2008. Noninvasive imaging of quantitative cerebral blood flow changes during 100% oxygen inhalation using arterial spin-labeling MR imaging. AJNR Am J Neuroradiol 29, 663–667.
Zappe, A.C., Uludag, K., Oeltermann, A., Ugurbil, K., Logothetis, N.K., 2008. The influence of moderate hypercapnia on neural activity in the anesthetized nonhuman primate. Cereb Cortex 18, 2666–2673.
Zhang, Y., Brady, M., Smith, S., 2001. Segmentation of brain MR images through a hidden Markov random field model and the expectation-maximization algorithm. IEEE Trans Med Imaging 20, 45–57.
Zysset, S., Schroeter, M.L., Neumann, J., von Cramon, D.Y., 2007. Stroop interference, hemodynamic response and aging: an event-related fMRI study. Neurobiol Aging 28, 937–946.